ACS Sustainable Chemistry & Engineering

pubs.acs.org/journal/ascecg

Research Article

Multi-Objective Optimization of a Hybrid Fossil/Renewable Carbon Methanol Cluster

Sachin Jog, Juan D. Medrano-García, Daniel Vázquez, and Gonzalo Guillén-Gosálbez*

Cite This: ACS Sustainable Chem. Eng. 2025, 13, 1473−1483

Read Online

ACCESS | Metrics & More | Article Recommendations | Supporting Information

ABSTRACT: Replacing fossil carbon- with renewable carbon-based technologies is imperative for transitioning to sustainable chemical production. However, most production pathways based on renewable carbon are currently economically unappealing. Here, we show that hybrid clusters exploiting synergies between different fossil and renewable carbon-based processes in terms of heat, mass, and power integration could make defossilized chemical technologies more competitive. We consider an integrated carbon cluster based on fossil and renewable carbon feedstocks for methanol production, including a novel oxy-combustion cycle for purge gas treatment and power generation. Using multiobjective optimization considering economic and environmental criteria (i.e., unitary production cost and global warming potential (GWP) impact, respectively), we find that integrated clusters could reduce the cost of carbon-neutral methanol by up to 30%, while leading to reductions in GWP impact from 21 to 142% for a given unitary production cost target, and heating utility savings between 80 and 100%. We conclude that hybridization of fossil and renewable technologies could become instrumental in enabling a gradual shift toward sustainable chemical production pathways.

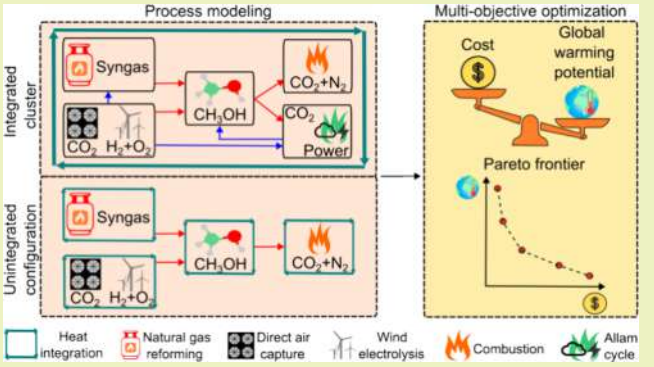

KEYWORDS: *climate change mitigation, integrated carbon cluster, multiobjective optimization, global warming potential, heat integration*

INTRODUCTION

The Paris Agreement[1] of 2015 has prompted worldwide efforts to limit the average temperature rise globally to well below 2 °C with reference to preindustrial levels, and to pursue further steps to limit it to 1.5 °C. Further, in the Conference of the Parties (COP) 26 (which took place in 2021, and led to the Glasgow Climate Pact[2]), countries committed to strive to limit the temperature rise to 1.5 °C to reduce the harmful effects of climate change. The chemical industry, which accounts for about 10% of anthropogenic greenhouse gas emissions globally,[3,4] heavily relies on fossil carbon.[5,6] Moreover, demand for chemicals is projected to rise significantly (e.g., methanol demand is expected to grow from 98 million tons (Mt) in 2021 to 500 Mt by 2050,[7] and ammonia demand from 185 Mt in 2020 to 355 Mt by 2050[8]). Therefore, continued dependence on fossil carbon alongside the demand rise will further increase the greenhouse gas emissions of the chemical industry. Thus, to meet the Paris Agreement, it is imperative for the chemical industry to move away from its reliance on fossil carbon.[9]

In this context, carbon capture and utilization (CCU), biomass utilization, and waste utilization are emerging as promising pathways for producing chemicals from renewable carbon. These alternatives are now being intensively investigated, mostly by applying process modeling and, more recently, life cycle assessment (LCA), and with a special focus on platform chemicals. For example, Kätelhön et al.[10] found that while CCU could reduce annual greenhouse gas emissions up to 3.5 gigatons CO_2-eq in 2030 (which were at 56 ± 6.6 gigatons CO_2-eq in 2019[11]), the additional operating cost could be up to 164% of the market value of chemicals. More specifically, Ioannou et al.[6] analyzed the economic and environmental performance of a CO_2 refinery (with CO_2 from direct air capture (DAC), and H_2 from water electrolysis powered by renewable energy), finding that while the refinery is not currently economically competitive, it could reduce up to 135% the global warming potential (GWP) impact compared to the fossil-based process. Biomass utilization was studied by Yang et al.,[12] performing a comparative techno-economic and LCA analysis of ethylene production using wet shale gas and biomass, concluding that while the GWP impact was 143% lower with the biomass-based route, its break-even price was at least 20% higher. Additionally, Yang et al.[13] studied aromatics production using fossil and biomass-based

Received: August 8, 2024
Revised: December 17, 2024
Accepted: December 18, 2024
Published: January 22, 2025

routes, showing that while none of the biomass routes were economically competitive with the fossil route, their greenhouse gas mitigation potential was between 86 and 102% relative to the fossil analog. Hydrogen production using waste polymer gasification with carbon capture and storage (CCS) was analyzed by Salah et al.,[14] concluding that while this route is more expensive than fossil- and biomass-based gasification, it shows superior environmental performance compared to fossil-based and most electrocatalytic routes.

As such, most of the previous studies on renewable carbon-based technologies analyzed them isolated from each other. However, here we argue that it is crucial to investigate synergies between various feedstocks and pathways to enable a more comprehensive evaluation of technologies. This could lead to the creation of an "eco-industrial park", mimicking the operation of natural ecosystems, i.e., optimizing mass and energy usage while minimizing waste through mass, heat, and power integration, common transport and waste disposal systems, etc.[15] This integration of technologies, focusing on fossil and renewable carbon feedstock, seems particularly appealing given their complementary strengths (cheaper fossil carbon routes, but less environmentally appealing relative to their renewable carbon counterparts).

In this regard, there have been several works investigating entire process networks following a superstructure-based optimization framework, using either linear programming (LP) or mixed integer linear programming (MILP) models and first-principles equations. While some studies focused exclusively on renewable routes for chemicals[16] and power production,[17,18] others integrated fossil and renewable carbon technologies. For example, using an LP model, Ioannou et al.[19] found that while renewable technologies for ethylene production are currently 1.7−3.9 times more expensive than their fossil counterparts, hybridization of fossil and renewable technologies could produce carbon-neutral ethylene with a 30% premium only (over current market prices). Demirhan et al.[20] developed an MILP model integrating fossil and renewable carbon technologies for a network of fuels, chemicals and power production, which achieved a cost reduction of at least 17%.

Several other works studied the efficiency improvements obtained through the integration of fossil and renewable carbon technologies using nonlinear process models. For example, Katayama and Tamaura[21] showed that carbon-neutral methanol could be produced at the same price as fossil methanol by combining solar-powered renewable energy for H_2 production with partial oxidation of coal and natural gas. Clausen et al.[22] showed that the best methanol energy efficiency was attained by a hybridization of autothermal biogas reforming and water electrolysis. Dongliang et al.[23] showed that supplementing the coal-to-methanol (CTM) process with green H_2 resulted in higher energy efficiency and methanol output, and lower CO_2 emissions than the conventional CTM process. Other works studied CO_2 abatement through a combination of captured CO_2 from fossil fuel plants and renewable H_2 or biomass, producing only methanol,[24−26] or coproducing power and methanol.[27−29] Further, multiple previous works have studied the coutilization of natural gas and biomass for CO_2 abatement, for example, methanol production using cogasification of natural gas and biomass,[30] the Hynol process,[31,32] and the modified Battelle-Columbus Laboratory (BCL) process.[33] Additionally, natural gas and biomass coutilization has been studied for the coproduction of methanol and electricity,[34] and polygeneration of synthetic fuels (including methanol) and electricity.[35,36] Using mixed integer nonlinear programming (MINLP) models for integrating technologies, Onel et al.[37] introduced a process synthesis and global optimization framework to coproduce liquid fuels and olefins from natural gas and biomass, showing that economies of scale make the integrated plant economically appealing. Baliban et al.[38,39] developed an MINLP framework for the thermochemical conversion of biomass, coal and natural gas to liquid transportation fuels, highlighting topological differences in the superstructure and the greenhouse gas emissions reduction potential.

Most of the works above either focused on single-objective optimization or failed to apply any optimization at all. Meanwhile, works applying multiobjective optimization using economic and environmental objective functions to integrated (nonlinear) process networks are scarce. With regards to linear superstructures, Ahmed et al.[40] developed an LP tool for multiobjective optimization of platform chemicals production in sustainable clusters, while Al-Mohannadi et al.[41] created a multiperiod multiobjective MILP model to analyze temporal carbon emissions reduction in integrated clusters. Concerning multiobjective optimization of integrated nonlinear process models, Fuentes-Cortés et al.[42] developed an MINLP model for the design of combined heat and power systems using natural gas and biogas feedstocks. Regarding chemical production, Noureldin and El-Halwagi[43] developed CHO-SYNs, i.e., C−H−O SYmbiosis Networks, based on a cluster of plants containing streams of C−H−O compounds and sharing centralized facilities. Panu et al.[44] used multiobjective optimization to design CHOSYNs for conversion of CO_2 to value-added chemicals, capturing substantial synergies between CO_2 sources and sinks.

In this work, we design and optimize an integrated cluster for methanol production and explore the hybridization of fossil and renewable carbon-based technologies using nonlinear superstructures. To our knowledge, this is the first work that applies multiobjective optimization to a network of nonlinear first-principles process models integrating fossil with renewable carbon technologies for chemical production. Additionally, we also incorporate a novel, high-pressure power generation cycle, i.e., the Allam cycle,[45] in the integrated cluster to showcase the additional benefits that can be attained via mass and power integration. Through the multiobjective optimization, we show the potential for hybridization between fossil and renewable carbon routes in terms of economic and environmental savings.

The structure of the paper is as follows. We first describe the problem statement, followed by details of the process modeling and multiobjective optimization. Next, we describe the results of the multiobjective optimization in terms of economic and environmental performance, followed by the conclusions of this work.

METHODS

In this section, we first describe the problem statement, followed by the modeling of each process, and the details of the multiobjective optimization.

Problem Statement and Overall Approach. We consider the methanol production process as the primary technology for our analysis. The feedstock can be a pure fossil source (i.e., syngas from the autothermal reforming (ATR) of natural gas), a pure renewable source (i.e., CO_2 from DAC, which will react with H_2 from water electrolysis using the solid oxide electrolytic cell (SOEC)), or a combination of both via hybridization of both routes. In addition, the

https://doi.org/10.1021/acssuschemeng.4c06566
ACS Sustainable Chem. Eng. 2025, 13, 1473−1483

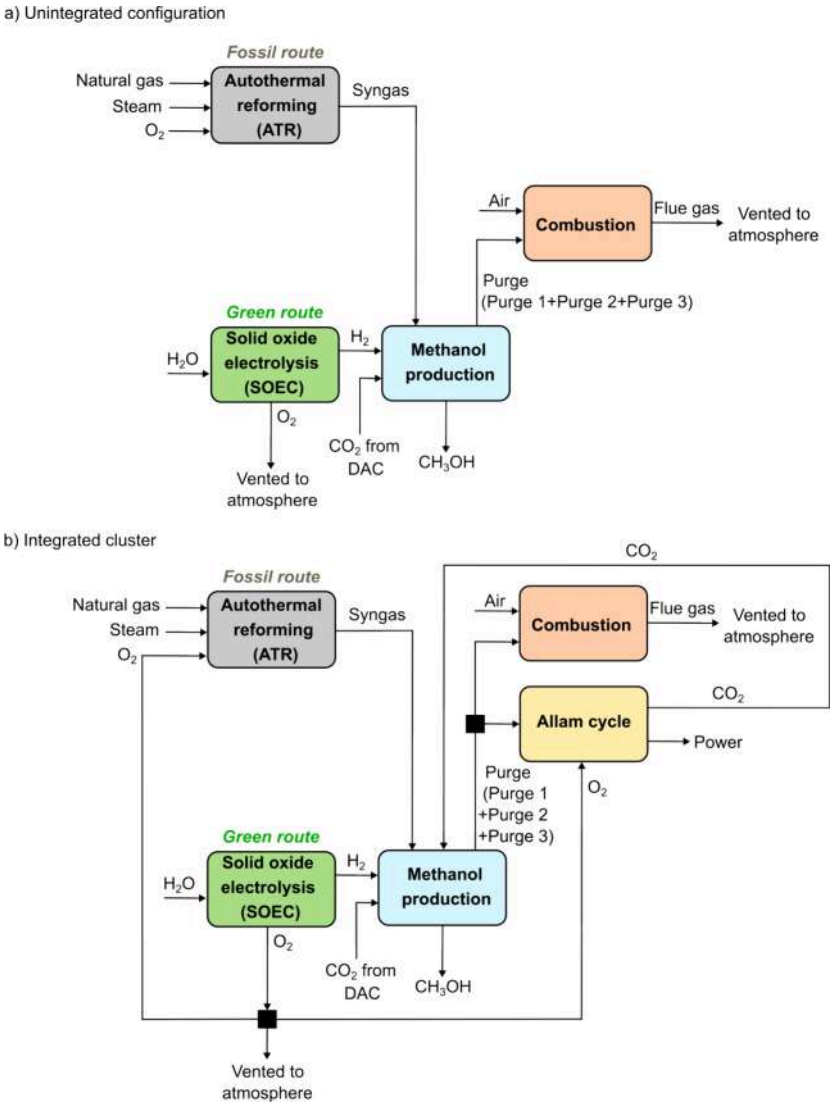

Figure 1. Process block diagrams of (a) unintegrated configuration and (b) integrated cluster.

purges from the methanol production process can be utilized in a combustion process, or in the Allam cycle. We first develop process models of these technologies, and then exploit their synergies considering heat, mass, and power integration. This integrated cluster is compared with an unintegrated configuration of the same processes that does not implement an Allam cycle. The aim of the analysis is to conduct a multiobjective optimization of the two process configurations to quantify their economic and environmental performance and showcase the benefits of exploiting process synergies in the integrated cluster. For this, we consider the unitary production cost (in $\$\cdot kg^{-1}$ of methanol) and GWP impact (in kg CO_2-eq$\cdot kg^{-1}$ of methanol) as the two objective functions. We also compare the unitary production cost required for carbon-neutral methanol production using the two process configurations. Finally, we show the potential for hybridization between the fossil and renewable carbon-based routes for a gradual transition to more sustainable methanol production.

Figure 1 shows the process block diagrams of the two configurations, while more detailed process flowsheets are shown in Section B of the Supporting Information.

Process Modeling. The unintegrated configuration (Figure 1a) consists of ATR, SOEC, methanol production and combustion, while the integrated cluster (Figure 1b) additionally includes the Allam cycle to exploit the synergies between the different processes. The SOEC is modeled using the Aspen Custom Modeler® (ACM) v11, while all other processes are modeled using available process units in Aspen HYSYS® v11. The following paragraphs briefly describe the modeling of each individual process, while we provide detailed descriptions in Section B of the Supporting Information.

The fossil-based route consists of the ATR process,[46] which utilizes natural gas, steam, and O_2 as feedstock. The feedstock is compressed (with intermediate cooling) and sent to the reactor, where methane reforming occurs. We then separate the resultant syngas (which consists of CO, H_2, and CO_2) from water using a flash unit, after cooling the reactor outlet. Finally, the syngas stream is compressed to the required pressure for methanol synthesis.

The renewable-based route utilizes the SOEC powered by wind electricity to produce H_2 and O_2. The SOEC is modeled based on the work by D'Angelo et al.,[47] in which an inlet water stream is heated up before entering the SOEC, where H_2 and O_2 are produced. The electrolysis products are cooled down, and unconverted water is separated from H_2 in a flash unit. This water is recycled to the inlet of the heater as a coolant for the electrolysis stack, eliminating the need for additional cooling. To achieve the high temperatures needed in the ATR and SOEC, we use natural gas as the heating utility, which can achieve temperatures of up to 2050 °C[48] during adiabatic combustion.

The methanol production process is based on the work by Vázquez and Guillén-Gosálbez.[49] The feed, which can either be from the fossil-based route, renewable-based route, or a combination of both routes,

https://doi.org/10.1021/acssuschemeng.4c06566
ACS Sustainable Chem. Eng. 2025, 13, 1473−1483

is preheated and sent to an adiabatic plug flow reactor (PFR) loaded with Cu−ZnO−Al_2O_3 catalyst. The reactor outlet is then cooled before entering the first flash unit, where most of the unreacted CO and H_2 are recompressed and recycled to the reactor inlet after a small fraction is purged (Purge 1). The liquid stream of the first flash unit is expanded before entering the second flash unit, where we separate a vapor purge stream (Purge 2). The liquid stream of the second flash unit is heated before being sent to a distillation column, which utilizes a partial vapor−liquid condenser, in which 99.9% pure methanol is obtained as the distillate, while a small amount of vapor product is purged (Purge 3). Note that in this analysis, the plant has a maximum theoretical methanol production capacity of 128 kilotons·year^{-1} due to the limitation associated with the stack size of SOECs (each SOEC stack has a capacity of 2.44 MW, producing 30 kmol·h^{-1} of H_2), while conventional methanol plants can have capacities up to 440 kilotons·year^{-1}.[50]

The three purge streams obtained from the methanol production process (Purge 1, Purge 2, and Purge 3 in Figure 1) are then combusted directly using 30% excess air, from which the flue gas (consisting mainly of CO_2, N_2, O_2, and H_2O, with a small quantity of CO) is vented into the atmosphere. Alternatively, the three purge streams can be utilized in an Allam cycle, which has been modeled based on the work by Ioannou et al.[6] The Allam cycle is a novel, high-pressure oxy-combustion cycle, which coproduces power and pure CO_2. Predominantly using hydrocarbon fuels as input, it consists of a semiclosed loop, high-pressure, low-pressure ratio recuperated Brayton cycle, using supercritical CO_2 as the working fluid. Thus, in the Allam cycle, the three purge streams are compressed to the same pressure and cofed with O_2 into an oxy-combustion burner. The produced flue gas is expanded to generate power, and the water content is removed using a flash unit. The vapor outlet of the flash unit leads to a 99.9% pure CO_2 stream, which can be recycled as feedstock to the methanol production process. However, most of the CO_2 is recycled to the inlet of the oxy-combustion reactor since the CO_2 is also acting as an inert gas for the oxy-combustion reaction to avoid a potential thermal runaway.

As previously mentioned, the integrated cluster aims to exploit the synergies between the different processes through heat, mass, and power integration. Therefore, the O_2 obtained from the SOEC is used as feed in the ATR and Allam cycle processes. Furthermore, the pure CO_2 obtained from the Allam cycle is partly recycled to the methanol production process, while the power produced in the Allam cycle is utilized in the other processes to satisfy their electricity requirements. Moreover, heat integration through the pinch methodology considers all process streams of all processes (i.e., ATR, SOEC, methanol production, and Allam cycle) simultaneously. However, in the unintegrated configuration, the O_2 for the ATR process and CO_2 for methanol production are purchased externally, and heat integration using the pinch methodology is only considered for each individual process (i.e., ATR, SOEC, and methanol production) separately. Here, we acknowledge that CCS is an option to reduce the impact of the flue gas stream that is combusted. However, we omit this option in both process configurations to be consistent with the business-as-usual (BAU) process. Moreover, this modeling choice simplifies the comparison with the Allam cycle in the integrated cluster. Further, we do not consider valorization of the O_2, since the current market demand is already covered by air separation, and its size is rather small compared to the methanol demand. The air separation process is especially essential for N_2 production (subsequently used for ammonia production). Therefore, assuming that there are no other surrounding industries which could use this O_2 for their own operations,[51,52] we vent it to the atmosphere. This venting does not result in any additional GWP impact on the process being considered.

Multiobjective Optimization. After modeling the two process configurations, we optimize the performance of the integrated cluster and unintegrated configuration separately, for which we employ multiobjective optimization using the ε-constraint method. Thus, the multiobjective problem is solved by computing a set of single objective problems as follows[53]:

$$\begin{aligned} &\min f_q(x, y) \\ \text{s. t.}\quad &f_j(x, y) \le \varepsilon_j \qquad \forall\, j \ne q \\ &h(x, y) = 0 \\ &g(x, y) \le 0 \\ &\underline{x} \le x \le \overline{x} \\ &x \in R^n,\ y \in \{0, 1\} \end{aligned} \tag{1}$$

where $f_q(x, y)$ is the objective function q that is optimized from the set J of objective functions, while all the others are transferred to additional constraints, imposing bounds on them. Parameters ε_j are then gradually varied to identify the Pareto optimal solutions of the problem.[54] Further, x and y denote the continuous and binary variables, respectively. The equality constraints are denoted by $h(x, y)$, while the inequality constraints are denoted by $g(x, y)$. The lower and upper bounds of the continuous variables are denoted by $\underline{x}$ and $\overline{x}$, respectively.

As mentioned previously, we consider two objective functions, i.e., unitary production cost (in \$·kg^{-1} of methanol) and GWP impact (in kg CO_2-eq·kg^{-1} of methanol), which are calculated using eqs 2 and 3, respectively:

$$\text{cost} = \frac{(C^{\text{Feed}} + C^{\text{Utilities}} + C^{\text{Electricity}} + C^{\text{Wastewater}} + C^{\text{CAPEX}})}{F^{\text{Methanol}}} \tag{2}$$

$$\text{GWP impact} = \frac{(I^{\text{Feed}} + I^{\text{Utilities}} + I^{\text{Electricity}} + I^{\text{Wastewater}} + I^{\text{Emissions}})}{F^{\text{Methanol}}} \tag{3}$$

where the cost (C, in \$·h^{-1}) and GWP impact (I, in kg CO_2-eq·h^{-1}) associated with raw materials, utilities, electricity and wastewater are denoted by C^{Feed}, I^{Feed}, $C^{\text{Utilities}}$, $I^{\text{Utilities}}$, $C^{\text{Electricity}}$, $I^{\text{Electricity}}$, $C^{\text{Wastewater}}$ and $I^{\text{Wastewater}}$, respectively. The economic assessment is performed for the year 2019. C^{CAPEX} represents the capital expenditures (CAPEX) associated with the SOEC, compressors, and reactors, for which we use the correlations from Towler and Sinnott.[55] We consider a plant lifetime of 10 years for the annualization of the CAPEX, as explained further in Section A of the Supporting Information. Heat exchangers were excluded from the CAPEX, since heat integration was carried out using the pinch methodology considering that the operating expenditures (OPEX) of the heat exchanger network (HEN) dominate its CAPEX. Similarly, the contribution of the materials of construction of the plant equipment in the GWP impact was omitted (only when computing the GWP, not in the cost calculations), as it is comparatively very small.[47] $I^{\text{Emissions}}$ denotes the GWP impact associated with the direct emissions to the atmosphere from the combustion process. F^{Methanol} refers to the methanol production rate in kg·h^{-1}. Furthermore, it should be noted that the terms described above include different contributors, e.g., the feed term (kmol·h^{-1}) consists of the feedstocks (i.e., CO_2, natural gas, O_2, and process water (Feed_{CO_2}, $\text{Feed}_{\text{Natural gas}}$, Feed_{O_2}, and $\text{Feed}_{\text{Process water}}$, respectively). The utilities (GJ·h^{-1}) consist of heating utility (natural gas) and cooling utility (cooling water) ($\text{Utilities}_{\text{Hot}}$ and $\text{Utilities}_{\text{Cold}}$, respectively), while electricity (GJ·h^{-1}) consists of grid and wind-powered electricity ($\text{Electricity}_{\text{Grid}}$ and $\text{Electricity}_{\text{SOEC}}$, respectively). The grid electricity is used for compressors and pumps, while wind-powered electricity is used for the SOEC only. We divide the CAPEX (\$·h^{-1}) into that for the SOEC, and that for all other equipment ($\text{CAPEX}_{\text{SOEC}}$ and $\text{CAPEX}_{\text{Other}}$, respectively) to show the contribution of the SOEC more clearly. Finally, the emissions (kg CO_2-eq·h^{-1}) consist of direct CO_2 and CO emissions (Emissions_{CO_2}, and Emissions_{CO}, respectively). Equations 4 to 8 show the individual terms for each component of the total cost and GWP impact:

https://doi.org/10.1021/acssuschemeng.4c06566
ACS Sustainable Chem. Eng. 2025, 13, 1473−1483

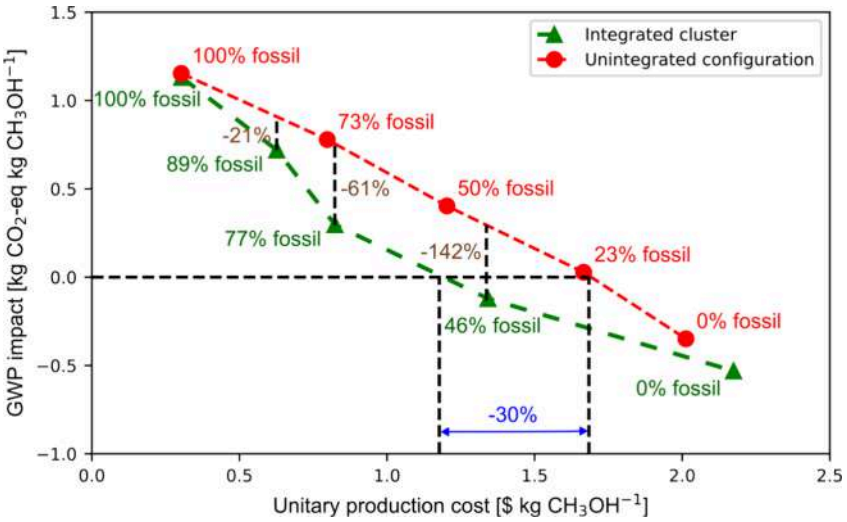

Figure 2. Pareto fronts of the integrated cluster and unintegrated configuration showing the hybridization (as the percentage of fossil route over the full integration), percentual improvement in GWP impact, and reduction in unitary cost for carbon-neutral methanol production in the integrated cluster.

$$C^{\text{Feed}} = C^{\text{Feed}}_{CO_2} + C^{\text{Feed}}_{\text{Natural gas}} + C^{\text{Feed}}_{O_2} + C^{\text{Feed}}_{\text{Process water}}$$
$$I^{\text{Feed}} = I^{\text{Feed}}_{CO_2} + I^{\text{Feed}}_{\text{Natural gas}} + I^{\text{Feed}}_{O_2} + I^{\text{Feed}}_{\text{Process water}} \quad (4)$$

$$C^{\text{Utilities}} = C^{\text{Utilities}}_{\text{Hot}} + C^{\text{Utilities}}_{\text{Cold}}$$
$$I^{\text{Utilities}} = I^{\text{Utilities}}_{\text{Hot}} + I^{\text{Utilities}}_{\text{Cold}} \quad (5)$$

$$C^{\text{Electricity}} = C^{\text{Electricity}}_{\text{Grid}} + C^{\text{Electricity}}_{\text{SOEC}}$$
$$I^{\text{Electricity}} = I^{\text{Electricity}}_{\text{Grid}} + I^{\text{Electricity}}_{\text{SOEC}} \quad (6)$$

$$C^{\text{CAPEX}} = C^{\text{CAPEX}}_{\text{Other}} + C^{\text{CAPEX}}_{\text{SOEC}} \quad (7)$$

$$I^{\text{Emissions}} = I^{\text{Emissions}}_{CO_2} + I^{\text{Emissions}}_{CO} \quad (8)$$

Concerning eq 3, we note that it follows the LCA principles. The functional unit corresponds to 1 kg of methanol. To compute the impact, we connect the mass and energy inputs from the technosphere to the foreground system with the corresponding life cycle emissions and impact via eco vectors, which are retrieved from Ecoinvent v3.8[56] and provide the life cycle impact per unit of reference flow. For example, in eq 5, $I^{\text{Utilities}}_{\text{Hot}}$ results from multiplying the amount of heating utility consumed by the plant with the GWP impact per unit of heating utility, where the latter is taken from Ecoinvent v3.8 and represents the product of the life cycle emissions per unit of heating utility and the corresponding characterization factors. Moreover, the impact of the direct emissions from the plant ($I^{\text{Emissions}}$ in eq 8) is computed from the flow of emissions and the corresponding characterization factors.

More specifically, for the GWP impact, we quantify the 100-year time horizon GWP (Hierarchist perspective) using the IPCC 2013 methodology[57] together with data from the Ecoinvent v3.8 cutoff database. Further details of the data used in the calculation of the two objective functions are described in Section A of the Supporting Information.

We use the algorithm *surrogateopt* from the Global Optimization Toolbox v4.6 in MATLAB® vR2021b,[58] which directly optimizes the flowsheet in Aspen HYSYS® v11 through the COM interface. This algorithm builds a surrogate model of the objective function through an interpolation of a cubic radial basis function. The surrogate model is then updated in each successive iteration of the optimization, based on the actual objective function value obtained from the flowsheet. Further details of the optimization procedure are described in Section C of the Supporting Information.

We consider eight degrees of freedom (all continuous variables) for the unintegrated configuration, and ten for the integrated cluster. One of the additional degrees of freedom of the integrated cluster, modeled with a binary variable, chooses between combustion and the Allam cycle for treating the process purge gas. The other additional degree of freedom of the integrated cluster is the temperature of the reactor feed of the Allam cycle. Thus, the optimization problem for the integrated cluster is posed as an MINLP problem, while that of the unintegrated configuration is a nonlinear programming (NLP) problem. The degrees of freedom and their associated ranges are shown in Section C of the Supporting Information.

It should be noted that to be consistent with the methanol production rate for each optimization run in both process configurations (integrated and unintegrated), we maintain the total amount of carbon entering the methanol production process (from the CH_4 in the fossil route, from the CO_2 in the renewable route, or the sum of CH_4 and CO_2 for a hybridization between both routes) equal to 5.00×10^2 kmol·h^{-1}. Thus, if we denote the natural gas molar flow rate by n kmol·h^{-1}, the CO_2 obtained from DAC is set to a value of $(5.00 \times 10^2 - n)$ kmol·h^{-1}.

Furthermore, we create a surrogate model for the SOEC based on Bayesian symbolic regression using the Bayesian Machine Scientist (BMS[59]). This is because the SOEC model in the ACM® v11 imported in Aspen HYSYS® v11 is found to be unstable when its input values (i.e., the degrees of freedom) are changed in successive iterations of the optimization, thus causing Aspen HYSYS® v11 to terminate abruptly. A detailed description of the BMS can be found elsewhere.[60] In essence, we use the BMS to generate an analytical model of the SOEC, which is then employed to enhance the numerical robustness of the overall optimization model. Additional details of the surrogate modeling using the BMS are provided in Section E of the Supporting Information.

RESULTS AND DISCUSSION

In this section, we discuss the Pareto fronts obtained from the multiobjective optimization, and analyze the economic and environmental results of each process configuration.

All calculations are performed on an Intel® Core i7 10700 CPU @ 2.90 GHz computer. The total time taken for generating the Pareto fronts for the integrated cluster and unintegrated configuration is 139,181 s and 84,848 s, respectively (i.e., about 38.66 and 23.57 h, respectively). The optimization of the integrated cluster is computationally more demanding because of the additional complexity of the

https://doi.org/10.1021/acssuschemeng.4c06566
ACS Sustainable Chem. Eng. 2025, 13, 1473−1483

flowsheet, and the inclusion of constraints to ensure that the CO_2 acting as inert for the oxy-combustion reaction in the Allam cycle is sufficient to prevent attaining a temperature beyond the upper limit. Further details of the multiobjective optimization are shown in Section C of the Supporting Information.

Multiobjective Optimization Results. The multiobjective optimization of the integrated cluster and unintegrated configuration for the minimization of unitary production cost and GWP impact yields the two Pareto fronts shown in Figure 2, with the integrated cluster dominating the unintegrated case. Note that the percentage of hybridization is given by the optimal results for the two process configurations. For each process configuration, the GWP impact is divided into equal intervals between the extreme points of the Pareto frontier, and the unitary production cost is optimized for the extremes of such intervals. This results in different hybridization configurations for the integrated cluster and unintegrated configuration. We now discuss the obtained Pareto fronts in terms of the process topologies, and other significant results showing the improved performance of the integrated cluster over the unintegrated configuration.

Process Topologies. We observe that the Allam cycle is selected for all Pareto points in the integrated cluster except for the minimum cost solution (i.e., 100% fossil route), which is due to the additional CAPEX contribution of the cycle. Thus, while the Allam cycle produces power and pure CO_2 (which is partly recycled as feed for methanol production), it is not advantageous in the minimum cost solution. This is because there is no CO_2 feed required, and power production using the Allam cycle is more expensive compared to grid electricity. Note that the process topology is the same for all Pareto points of the unintegrated configuration, i.e., they always implement combustion for purge utilization.

Characteristics of the Pareto fronts. Note that in what follows, we first show the integrated cluster values followed by the unintegrated configuration values. Overall, for both the integrated cluster and the unintegrated configuration, using the 100% fossil route (i.e., the optimized natural gas feedstock molar flow is equal to the upper bound, or 5.00×10^2 kmol·h^{-1}) results in lower costs (86−85%) and higher impacts (313−431%) compared to the minimum impact solution. The latter implements a completely renewable configuration (i.e., the optimized natural gas feedstock molar flow is 0 kmol·h^{-1}). This performance is due to the high cost of electrolytic H_2 and the negative impact contribution of DAC CO_2 due to carbon removal, as previously reported by some studies.[49,50,52]

The intermediate Pareto points show a gradual decrease in impact from the minimum cost with 100% fossil feedstock (1.13−1.15 kg CO_2-eq·kg^{-1}) to the minimum impact with 0% fossil feedstock (-5.31×10^{-1} to -3.49×10^{-1} kg CO_2-eq·kg^{-1}), based on the degree of hybridization. On the other hand, the economic performance behaves in the opposite manner, increasing from 3.04×10^{-1}−3.03×10^{-1} \$·kg^{-1} in the 100% fossil to 2.17−2.01 \$·kg^{-1} in the 0% fossil configuration.

Comparing the extreme points of the Pareto fronts, we observe that for the minimum cost solutions, both configurations exclusively choose the fossil route, with virtually the same unitary cost (the 0.3% difference in the integrated cluster is due to a lesser quantity of methanol being produced in it compared to the unintegrated configuration), and a 2% lower GWP impact in the integrated cluster. Both minimum cost solutions choose combustion for purge utilization, where the reduction in GWP impact of the integrated cluster is due to heat integration between all processes together. The contribution of heating utility to the unitary cost is negligible, hence not resulting in any significant difference in the unitary costs of the two configurations.

For the minimum GWP impact solutions, both configurations exclusively choose the green route, with the integrated cluster having an 8% higher unitary cost, and a 52% lower GWP impact than the unintegrated configuration. Further, as shown in Figure 2, for a given unitary cost target (defined as the intermediate Pareto points of the integrated cluster), the percentage improvement in the GWP impact for the integrated cluster with respect to the unintegrated configuration is 21, 61, and 142% for the Pareto points associated with 89, 77 and 46% fossil configurations. The percentage improvement in the GWP impact is greater than 100% for the configuration whose feed contains 46% of fossil feedstock. This happens because the unintegrated configuration has a positive GWP impact for this case (i.e., 2.91×10^{-1} kg CO_2-eq·kg^{-1}), while the integrated cluster has a negative GWP impact (i.e., -1.21×10^{-1} kg CO_2-eq·kg^{-1}), leading to a percentage improvement above 100%. Moreover, the negative GWP impact obtained in the integrated cluster is due to the cradle-to-gate scope of the LCA. This improvement in the GWP impact is due to the incorporation of the Allam cycle, which prevents direct CO_2 emissions due to mass integration (as the pure CO_2 is partly recycled as feed for methanol production), and lowers grid electricity requirements due to power integration. Moreover, the heat integration between all processes results in lower utility requirements, while mass integration results in reduced external O_2 requirement, further reducing the GWP impact. On the other hand, the 8% higher unitary cost of the integrated cluster in the minimum GWP impact solution is due to the additional CAPEX associated with the Allam cycle. This value is higher than the savings obtained from lower grid electricity, heating utility, CO_2 feed and O_2 feed requirements in the integrated cluster, thus resulting in a higher overall unitary cost.

Cost of Carbon-Neutral Methanol Production. We focus now on understanding the implications of integrating processes for attaining net-zero carbon emissions (cradle-to-gate) in methanol production. To this end, we analyzed the impact of the process configuration on the production of carbon-neutral methanol (i.e., zero GWP impact). As shown in Figure 2, we find that the integrated cluster can produce carbon-neutral methanol at a 30% lower cost than the unintegrated configuration. Compared to the unintegrated configuration, this cheaper cost in the integrated cluster is due to the incorporation of the Allam cycle, which results in lower grid electricity requirements, and prevents direct CO_2 emissions, while allowing for a higher contribution of fossil-based carbon feedstock for methanol production (and thus, a lower cost compared to the renewable carbon-based feed). Further, as explained previously, the heat and mass integration in the integrated cluster also result in cost savings.

Impact of Heat Integration. As mentioned previously, we use pinch technology to calculate the minimum heating and cooling utilities' targets for all processes together in the integrated cluster, and for each process individually in the unintegrated configuration. This results in significant utility savings in the integrated cluster. For the 100 and 89% fossil configurations of the integrated cluster, we observe 100%

https://doi.org/10.1021/acssuschemeng.4c06566
ACS Sustainable Chem. Eng. 2025, 13, 1473−1483

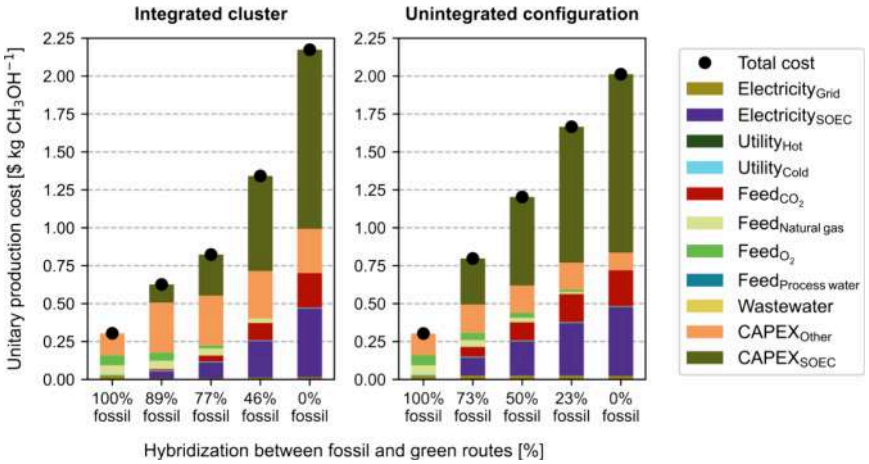

Figure 3. Breakdown of the unitary production cost for each Pareto point of the integrated cluster and unintegrated configuration. Individual terms are defined in eqs 2 to 8. The subscript "Other" refers to all process units but the SOEC. Wind electricity is assumed to be used only in the SOEC, while grid electricity is used in the rest of the plant.

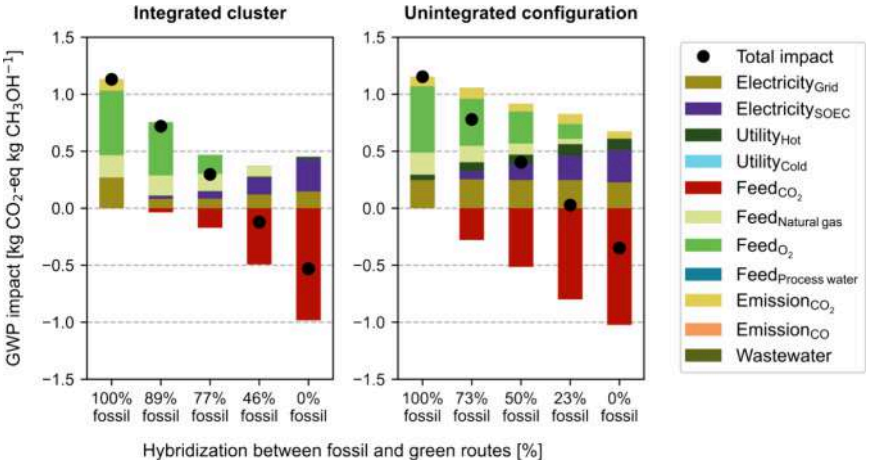

Figure 4. Breakdown of the GWP impact for each Pareto point of the integrated cluster and unintegrated configuration. Individual terms are defined in eqs 2 to 8. Wind electricity is assumed to be used only in the SOEC, while grid electricity is used in the rest of the plant.

heating utility savings compared to the 100 and 73% fossil configurations of the unintegrated configuration, while the 77, 46, and 0% fossil configurations have 96, 93, and 80% heating utility savings compared to the respective designs of the unintegrated configuration (i.e., 50, 23, and 0% fossil configurations), respectively. The significance of this reduction is most noticeable in the GWP impact, as discussed later in the Environmental Results.

Economic Results. Figure 3 shows the breakdown of the unitary production cost for each solution on the Pareto front for both process configurations. The respective values of individual contributions are shown in Section D of the Supporting Information. Notably, we can see from Figure 3 that for the 100% fossil route (i.e., the minimum cost solution), $CAPEX_{Other}$ (i.e., the capital cost of all process units but the SOEC) is the major cost contributor in both process configurations (47% for the integrated and unintegrated processes, from a total cost of 3.04×10^{-1} and 3.03×10^{-1} $\$\cdot kg^{-1}$, respectively). As explained earlier, since the methanol production plant has a lower capacity (128 kilotons·$year^{-1}$) than conventional plants (440 kilotons·$year^{-1}$), the relative contribution of the CAPEX to the unitary production cost is larger compared to conventional plants owing to economies of scale and the concave nature of the CAPEX correlations. The next important contributors are the natural gas feed cost, and the O_2 feed cost for the ATR, contributing approximately 20 and 22%, respectively in both processes, while grid electricity contributes around 9% to the total cost. As there is heat integration between all processes in the integrated cluster, the heating and cooling utilities together contribute less than 2% to the total cost, while this contribution increases to 3% in the unintegrated configuration. Thus, as the contribution of heating and cooling utilities to the unitary production cost is minor, heat integration does not reduce the cost significantly in the integrated cluster.

For the 0% fossil route (i.e., the minimum GWP impact solution), the CAPEX for the SOEC and its associated electricity consumption (i.e., the overall cost of H_2) are the major contributors to the cost (54 and 21%, respectively for the integrated cluster, which has a total cost of 2.17 $\$\cdot kg^{-1}$, and 58 and 22%, respectively for the unintegrated configuration, which has a total cost of 2.01 $\$\cdot kg^{-1}$). Thus, the overall cost of H_2 from wind-powered water electrolysis using the SOEC is 8.29 $\$\cdot kg^{-1}$ of H_2, which translates to 1.63 $\$\cdot kg^{-1}$ of methanol, for both process configurations. This value is in close agreement with the projected maximum cost of H_2 from

https://doi.org/10.1021/acssuschemeng.4c06566
ACS Sustainable Chem. Eng. 2025, 13, 1473−1483

wind-powered water electrolysis (with externalities) using the SOEC in 2030 (i.e., 8.10 $\$\cdot kg^{-1}$ of H_2), as reported by González-Garay et al.[50] Differences in the cost projections from various sources are mainly caused by uncertainties in the CAPEX of the SOEC due to the lack of actual investment cost data, which results from the limited number of SOEC installations until date.[61] The other two significant contributors to the cost are the rest of the CAPEX ($CAPEX_{Other}$) and the CO_2 feed cost. However, in the integrated cluster, the CO_2 feed has a lower impact on the cost due to CO_2 recycling.

Notably, for the hybridized production routes, the trend described for the extreme Pareto points remains the same. As expected, the contribution of the SOEC (both, $CAPEX_{SOEC}$ and wind electricity) progressively increases, while the relative contribution of $CAPEX_{Other}$ decreases. As the ATR process is gradually less favored, the contribution of the natural gas feed becomes less important, while that of the CO_2 feed increases as the SOEC process becomes more favorable. The contribution of heating utility, process water, and wastewater as a whole is less than 1% of the total cost for both process configurations.

Finally, the effect of carbon pricing on the economic evaluation is discussed in Section F of the Supporting Information.

Environmental Results. Figure 4 shows the breakdown of the GWP impact for each solution on the Pareto front for both process configurations. The respective values of individual contributions are shown in Section D of the Supporting Information. For the 100% fossil route (i.e., the minimum cost solution), the O_2 needed for the ATR process is the major contributor to the total positive GWP impact in both process configurations (50% each, from a total positive GWP impact of 1.13 and 1.15 $kg\text{-}CO_2\text{-}eq\cdot kg^{-1}$ for the integrated and unintegrated configurations, respectively). This is because we consider that O_2 is produced via cryogenic air separation, which consumes large amounts of electricity. The next significant contributors are the grid electricity (24−21%), natural gas feed (17% each), and the direct CO_2 emissions from the combustion process (9−7%). Significantly, as there is heat integration between all processes in the integrated cluster, there is no heating utility required, but it contributes 4% to the positive GWP impact in the unintegrated configuration.

For the 0% fossil route (i.e., the minimum GWP impact solution), the wind (SOEC) and grid (rest of the process) electricity consumption are the major contributors to the GWP impact in both configurations (95% of a total positive GWP impact of 4.53×10^{-1} $kg\text{-}CO_2\text{-}eq\cdot kg^{-1}$ for the integrated cluster, and 76% of a total positive GWP impact of 6.74×10^{-1} $kg\text{-}CO_2\text{-}eq\cdot kg^{-1}$ for the unintegrated configuration). The heating utility and the CO_2 emitted by the combustion process contribute more to the total impact in the unintegrated case relative to the integrated one (15 and 9%, respectively vs 5 and 0%, respectively for the integrated cluster). This is because the Allam cycle does not lead to any direct CO_2 emissions, and the integrated cluster requires much less heating utility because heat integration is further exploited. Moreover, as expected, the CO_2 obtained from DAC shows a negative contribution to the total GWP impact in both cases.

Further, for the hybridized production routes, as the renewable route becomes increasingly dominant, the contributions of the natural gas and O_2 feed decrease gradually, while those of the SOEC electricity and CO_2 feed (larger negative values) become more relevant. Considering the positive contributions to the GWP impact, the heating utility contributes between 4 and 15% in the unintegrated configuration, while it only contributes between 0 and 5% in the integrated cluster. The other components (cooling utility, direct CO emissions, process water, and wastewater) represent less than 1% of the total positive impact for both process configurations. Overall, for both process configurations, grid electricity (for all processes), wind electricity (for the SOEC), natural gas and oxygen feedstock (for the ATR), and the direct CO_2 emissions (from the combustion process) contribute the most to the GWP impact. As explained earlier, their relative contributions change depending on the hybridization level. Additionally, the heating utility significantly contributes to the GWP impact in the unintegrated configuration.

CONCLUSIONS

In this work, we studied the synergistic effects of integrating fossil and renewable carbon-based processes for methanol production based on mass, heat, and power integration, while considering a novel high-pressure, oxy-combustion technology, i.e., the Allam cycle. We used multiobjective optimization to compare the integrated cluster with an unintegrated process configuration considering economic and environmental criteria (unitary production cost and GWP impact, respectively).

We found that heat, mass, and power integration in the integrated cluster resulted in 30% cheaper carbon-neutral methanol, and reduced the GWP impact between 21 and 142% compared to the unintegrated configuration for a given unitary cost target. Additionally, the integrated cluster resulted in savings in heating utility ranging from 80 to 100%. Furthermore, while the minimum cost and GWP impact solutions exclusively chose only the fossil and renewable routes for methanol production respectively, our results showed the advantages of hybridization between such routes in the integrated cluster, decreasing the carbon footprint as much as 142% with 46% fossil feedstock usage.

Overall, our work showcases the advantages of integrating fossil and renewable carbon production pathways in the pursuit of climate change mitigation, which could enable a gradual transition to a more sustainable chemical industry.

ASSOCIATED CONTENT

Supporting Information

The Supporting Information is available free of charge at https://pubs.acs.org/doi/10.1021/acssuschemeng.4c06566.

Data for the economic and environmental evaluation, process simulations, additional details and results of the multiobjective optimization, breakdown of the costs and GWP impacts, the surrogate modeling results, and the effect of carbon pricing on the economic analysis (PDF)

AUTHOR INFORMATION

Corresponding Author

Gonzalo Guillén-Gosálbez − *Institute for Chemical and Bioengineering, Department of Chemistry and Applied Biosciences, ETH Zurich, 8093 Zurich, Switzerland;* orcid.org/0000-0001-6074-8473; Email: gonzalo.guillen.gosalbez@chem.ethz.ch

Authors

Sachin Jog − *Institute for Chemical and Bioengineering, Department of Chemistry and Applied Biosciences, ETH*

https://doi.org/10.1021/acssuschemeng.4c06566
ACS Sustainable Chem. Eng. 2025, 13, 1473−1483

Zurich, 8093 Zurich, Switzerland; orcid.org/0000-0003-3927-4036

Juan D. Medrano-García − *Institute for Chemical and Bioengineering, Department of Chemistry and Applied Biosciences, ETH Zurich, 8093 Zurich, Switzerland;* orcid.org/0000-0001-5422-1683

Daniel Vázquez − *IQS School of Engineering, Universitat Ramon Llull, 08017 Barcelona, Spain;* orcid.org/0000-0001-9380-3918

Complete contact information is available at: https://pubs.acs.org/10.1021/acssuschemeng.4c06566

Author Contributions

The manuscript was written through contributions of all authors. All authors have given approval to the final version of the manuscript.

Notes

The authors declare no competing financial interest.

■ ACKNOWLEDGMENTS

The authors would like to acknowledge the financial support from the Swiss National Science Foundation (Project LEARN-D, MINT 200021_214877). D.V. and J.D.M-G. acknowledge support from grant PID2023-151826OA-I00 funded by MICIU/AEI/10.13039/501100011033 and ERDF/EU.

■ ABBREVIATIONS

ACM, Aspen Custom Modeler; ATR, autothermal reforming; BAU, business-as-usual; BCL, Battelle-Columbus Laboratory; BMS, Bayesian Machine Scientist; CAPEX, capital expenditures; CCS, carbon capture and storage; CCU, carbon capture and utilization; COP, Conference of the Parties; CTM, coal-to-methanol; DAC, direct air capture; GWP, global warming potential; HEN, heat exchanger network; LCA, life cycle assessment; LP, linear programming; MILP, mixed integer linear programming; MINLP, mixed integer nonlinear programming; Mt, million tons; NLP, nonlinear programming; OPEX, operating expenditures; PFR, plug flow reactor; SOEC, solid oxide electrolytic cell

■ SUBSCRIPTS

$j \in J$, objective functions; $q \in J$, objective function to be optimized.

■ PARAMETERS

ε_j, parameters in the epsilon-constraint method

■ VARIABLES

x, Continuous variables; y, Binary variables; C^{Feed}, Cost of feedstock [$\$\cdot h^{-1}$]; $C^{\text{Utilities}}$, Cost of utilities [$\$\cdot h^{-1}$]; $C^{\text{Electricity}}$, Cost of electricity [$\$\cdot h^{-1}$]; $C^{\text{Wastewater}}$, Cost of wastewater treatment [$\$\cdot h^{-1}$]; C^{CAPEX}, Capital cost [$\$\cdot h^{-1}$]; I^{Feed}, GWP impact of feedstock [kg CO_2-eq$\cdot h^{-1}$]; $I^{\text{Utilities}}$, GWP impact of utilities [kg CO_2-eq$\cdot h^{-1}$]; $I^{\text{Electricity}}$, GWP impact of electricity [kg CO_2-eq$\cdot h^{-1}$]; $I^{\text{Wastewater}}$, GWP impact of wastewater treatment [kg CO_2-eq$\cdot h^{-1}$]; $I^{\text{Emissions}}$, GWP impact of emissions to the atmosphere [kg CO_2-eq$\cdot h^{-1}$]; $C^{\text{Feed}}_{CO_2}$, Cost of CO_2 feed [$\$\cdot h^{-1}$]; $C^{\text{Feed}}_{\text{Natural gas}}$, Cost of natural gas feed [$\$\cdot h^{-1}$]; $C^{\text{Feed}}_{O_2}$, Cost of O_2 feed [$\$\cdot h^{-1}$]; $C^{\text{Feed}}_{\text{Process water}}$, Cost of process water feed [$\$\cdot h^{-1}$]; $C^{\text{Utilities}}_{\text{Hot}}$, Cost of heating utility [$\$\cdot h^{-1}$]; $C^{\text{Utilities}}_{\text{Cold}}$, Cost of cooling utility [$\$\cdot h^{-1}$]; $C^{\text{Electricity}}_{\text{Other}}$, Cost of electricity for the compressors and pumps [$\$\cdot h^{-1}$]; $C^{\text{Electricity}}_{\text{SOEC}}$, Cost of electricity for the SOEC [$\$\cdot h^{-1}$]; $C^{\text{CAPEX}}_{\text{Other}}$, Capital cost of compressors and reactors [$\$\cdot h^{-1}$]; $C^{\text{CAPEX}}_{\text{SOEC}}$, Capital cost of SOEC [$\$\cdot h^{-1}$]; $I^{\text{Feed}}_{CO_2}$, GWP impact of CO_2 feed [kg CO_2-eq$\cdot h^{-1}$]; $I^{\text{Feed}}_{\text{Natural gas}}$, GWP impact of natural gas feed [kg CO_2-eq$\cdot h^{-1}$]; $I^{\text{Feed}}_{O_2}$, GWP impact of O_2 feed [kg CO_2-eq$\cdot h^{-1}$]; $I^{\text{Feed}}_{\text{Process water}}$, GWP impact of process water feed [kg CO_2-eq$\cdot h^{-1}$]; $I^{\text{Utilities}}_{\text{Hot}}$, GWP impact of heating utility [kg CO_2-eq$\cdot h^{-1}$]; $I^{\text{Utilities}}_{\text{Cold}}$, GWP impact of cooling utility [kg CO_2-eq$\cdot h^{-1}$]; $I^{\text{Electricity}}_{\text{Other}}$, GWP impact of electricity used in compressors and pumps [kg CO_2-eq$\cdot h^{-1}$]; $I^{\text{Electricity}}_{\text{SOEC}}$, GWP impact of electricity used in SOEC [kg CO_2-eq$\cdot h^{-1}$]; $I^{\text{Emissions}}_{CO_2}$, GWP impact of CO_2 emissions to the atmosphere [kg CO_2-eq$\cdot h^{-1}$]; $I^{\text{Emissions}}_{CO}$, GWP impact of CO emissions to the atmosphere [kg CO_2-eq$\cdot h^{-1}$]; F^{Methanol}, methanol production rate [$kg\cdot h^{-1}$]

■ REFERENCES

(1) United Nations. *Framework Convention on Climate Change (UNFCCC)*; Paris Agreement: United Nations, 2016. https://unfccc.int/process-and-meetings/the-paris-agreement/the-paris-agreement (accessed June 14, 2024).

(2) United Nations. *Framework Convention on Climate Change (UNFCCC), Outcomes of the Glasgow Climate Change Conference - Advance Unedited Versions (AUVs)*; UN Campus: Bonn, Germany, 2021. https://unfccc.int/ (accessed October 22, 2024).

(3) Bauer, F.; Kulionis, V.; Oberschelp, C.; Pfister, S.; Tilsted, J. P.; Finkill, G. D.; Fjäll, S. *Petrochemicals and Climate Change: Tracing Globally Growing Emissions and Key Blind Spots in a Fossil-Based Industry*, 2022.

(4) Bauer, F.; Tilsted, J. P.; Pfister, S.; Oberschelp, C.; Kulionis, V. Mapping GHG Emissions and Prospects for Renewable Energy in the Chemical Industry. *Curr. Opin. Chem. Eng.* **2023**, *39*, 100881.

(5) Nabera, A.; Istrate, I.-R.; Martín, A. J.; Pérez-Ramírez, J.; Guillén-Gosálbez, G. Energy Crisis in Europe Enhances the Sustainability of Green Chemicals. *Green Chem.* **2023**, *25* (17), 6603−6611.

(6) Ioannou, I.; Javaloyes-Antón, J.; Caballero, J. A.; Guillén-Gosálbez, G. Economic and Environmental Performance of an Integrated CO_2 Refinery. *ACS Sustain. Chem. Eng.* **2023**, *11* (5), 1949−1961.

(7) IRENA. *Innovation Outlook: Renewable Methanol*; Abu Dhabi, 2021. http://www.irena.org/.

(8) IEA. *Ammonia Technology Roadmap: Towards More Sustainable Nitrogen Fertiliser Production*, 2021.

(9) Galán-Martín, Á.; Vázquez, D.; Cobo, S.; Mac Dowell, N.; Caballero, J. A.; Guillén-Gosálbez, G. Delaying Carbon Dioxide Removal in the European Union Puts Climate Targets at Risk. *Nat. Commun.* **2021**, *12* (1), 6490.

(10) Kätelhön, A.; Meys, R.; Deutz, S.; Suh, S.; Bardow, A. Climate Change Mitigation Potential of Carbon Capture and Utilization in the Chemical Industry. *Proc. Natl. Acad. Sci. U. S. A.* **2019**, *116* (23), 11187−11194.

(11) IPCC. Summary for Policymakers. In *Climate Change 2022 - Mitigation of Climate Change Contribution of Working Group III to the Sixth Assessment Report of the Intergovernmental Panel on Climate Change*; Cambridge University Press, 2023; pp 3−48.

(12) Yang, M.; Tian, X.; You, F. Manufacturing Ethylene from Wet Shale Gas and Biomass: Comparative Technoeconomic Analysis and Environmental Life Cycle Assessment. *Ind. Eng. Chem. Res.* **2018**, *57* (17), 5980−5998.

(13) Yang, F.; Meerman, H.; Zhang, Z.; Jiang, J.; Faaij, A. Integral Techno-Economic Comparison and Greenhouse Gas Balances of Different Production Routes of Aromatics from Biomass with CO_2 Capture. *J. Clean. Prod.* **2022**, *372*, 133727.

(14) Salah, C.; Cobo, S.; Pérez-Ramírez, J.; Guillén-Gosálbez, G. Environmental Sustainability Assessment of Hydrogen from Waste Polymers. *ACS Sustain. Chem. Eng.* **2023**, *11* (8), 3238−3247.

(15) Butturi, M. A.; Lolli, F.; Sellitto, M. A.; Balugani, E.; Gamberini, R.; Rimini, B. Renewable Energy in Eco-Industrial Parks and Urban-Industrial Symbiosis: A Literature Review and a Conceptual Synthesis. *Appl. Energy* **2019**, *255*, 113825.
(16) Martín, M.; Grossmann, I. E. Optimal Integration of a Self Sustained Algae Based Facility with Solar and/or Wind Energy. *J. Clean. Prod.* **2017**, *145*, 336−347.
(17) Martín, M.; Grossmann, I. E. Optimal Integration of Renewable Based Processes for Fuels and Power Production: Spain Case Study. *Appl. Energy* **2018**, *213*, 595−610.
(18) Zhang, Q.; Martín, M.; Grossmann, I. E. Integrated Design and Operation of Renewables-Based Fuels and Power Production Networks. *Comput. Chem. Eng.* **2019**, *122*, 80−92.
(19) Ioannou, I.; D'Angelo, S. C.; Martín, A. J.; Pérez-Ramírez, J.; Guillén-Gosálbez, G. Hybridization of Fossil- and CO_2-Based Routes for Ethylene Production Using Renewable Energy. *ChemSusChem* **2020**, *13* (23), 6370−6380.
(20) Demirhan, C. D.; Tso, W. W.; Powell, J. B.; Pistikopoulos, E. N. A Multi-Scale Energy Systems Engineering Approach towards Integrated Multi-Product Network Optimization. *Appl. Energy* **2021**, *281*, 116020.
(21) Katayama, Y.; Tamaura, Y. Development of New Green-Fuel Production Technology by Combination of Fossil Fuel and Renewable Energy. *Energy* **2005**, *30* (11−12), 2179−2185.
(22) Clausen, L. R.; Houbak, N.; Elmegaard, B. Technoeconomic Analysis of a Methanol Plant Based on Gasification of Biomass and Electrolysis of Water. *Energy* **2010**, *35* (5), 2338−2347.
(23) Dongliang, W.; Wenliang, M.; Huairong, Z.; Guixian, L.; Yong, Y.; Hongwei, L. Green Hydrogen Coupling with CO_2 Utilization of Coal-to-Methanol for High Methanol Productivity and Low CO_2 Emission. *Energy* **2021**, *231*, 120970.
(24) Hank, C.; Gelpke, S.; Schnabl, A.; White, R. J.; Full, J.; Wiebe, N.; Smolinka, T.; Schaadt, A.; Henning, H.-M.; Hebling, C. Economics & Carbon Dioxide Avoidance Cost of Methanol Production Based on Renewable Hydrogen and Recycled Carbon Dioxide−Power-to-Methanol. *Sustain. Energy Fuels* **2018**, *2* (6), 1244−1261.
(25) Abad, D.; Vega, F.; Navarrete, B.; Delgado, A.; Nieto, E. Modeling and Simulation of an Integrated Power-to-Methanol Approach via High Temperature Electrolysis and Partial Oxy-Combustion Technology. *Int. J. Hydrogen Energy* **2021**, *46* (69), 34128−34147.
(26) Lundgren, J.; Ekbom, T.; Hulteberg, C.; Larsson, M.; Grip, C.-E.; Nilsson, L.; Tunå, P. Methanol Production from Steel-Work off-Gases and Biomass Based Synthesis Gas. *Appl. Energy* **2013**, *112*, 431−439.
(27) Soltanieh, M.; Azar, K. M.; Saber, M. Development of a Zero Emission Integrated System for Co-Production of Electricity and Methanol through Renewable Hydrogen and CO_2 Capture. *Int. J. Greenh. Gas Control* **2012**, *7*, 145−152.
(28) Mignard, D. Methanol Synthesis from Flue-Gas CO_2 and Renewable Electricity: A Feasibility Study. *Int. J. Hydrogen Energy* **2003**, *28* (4), 455−464.
(29) Nazerifard, R.; Khani, L.; Mohammadpourfard, M.; Mohammadi-Ivatloo, B.; Akkurt, G. G. Design and Thermodynamic Analysis of a Novel Methanol, Hydrogen, and Power Trigeneration System Based on Renewable Energy and Flue Gas Carbon Dioxide. *Energy Convers. Manag.* **2021**, *233*, 113922.
(30) Chmielniak, T.; Sciazko, M. Co-Gasification of Biomass and Coal for Methanol Synthesis. *Appl. Energy* **2003**, *74* (3−4), 393−403.
(31) Dong, Y.; Steinberg, M. Hynol−An Economical Process for Methanol Production from Biomass and Natural Gas with Reduced CO_2 Emission. *Int. J. Hydrogen Energy* **1997**, *22* (10−11), 971−977.
(32) Borgwardt, R. H. Biomass and Natural Gas as Co-Feedstocks for Production of Fuel for Fuel-Cell Vehicles. *Biomass and Bioenergy* **1997**, *12* (5), 333−345.
(33) Borgwardt, R. H. Methanol Production from Biomass and Natural Gas as Transportation Fuel. *Ind. Eng. Chem. Res.* **1998**, *37* (9), 3760−3767.
(34) Li, H.; Hong, H.; Jin, H.; Cai, R. Analysis of a Feasible Polygeneration System for Power and Methanol Production Taking Natural Gas and Biomass as Materials. *Appl. Energy* **2010**, *87* (9), 2846−2853.
(35) Adams, T. A.; Barton, P. I. Combining Coal Gasification, Natural Gas Reforming, and Solid Oxide Fuel Cells for Efficient Polygeneration with CO_2 Capture and Sequestration. *Fuel Process. Technol.* **2011**, *92* (10), 2105−2115.
(36) Liu, G.; Williams, R. H.; Larson, E. D.; Kreutz, T. G. Design/Economics of Low-Carbon Power Generation from Natural Gas and Biomass with Synthetic Fuels Co-Production. *Energy Procedia* **2011**, *4*, 1989−1996.
(37) Onel, O.; Niziolek, A. M.; Elia, J. A.; Baliban, R. C.; Floudas, C. A. Biomass and Natural Gas to Liquid Transportation Fuels and Olefins (BGTL+C2_C4): Process Synthesis and Global Optimization. *Ind. Eng. Chem. Res.* **2015**, *54* (1), 359−385.
(38) Baliban, R. C.; Elia, J. A.; Floudas, C. A. Optimization Framework for the Simultaneous Process Synthesis, Heat and Power Integration of a Thermochemical Hybrid Biomass, Coal, and Natural Gas Facility. *Comput. Chem. Eng.* **2011**, *35* (9), 1647−1690.
(39) Baliban, R. C.; Elia, J. A.; Floudas, C. A. Simultaneous Process Synthesis, Heat, Power, and Water Integration of Thermochemical Hybrid Biomass, Coal, and Natural Gas Facilities. *Comput. Chem. Eng.* **2012**, *37*, 297−327.
(40) Ahmed, R. O.; Al-Mohannadi, D. M.; Linke, P. Multi-Objective Resource Integration for Sustainable Industrial Clusters. *J. Clean. Prod.* **2021**, *316*, 128237.
(41) Al-Mohannadi, D. M.; Linke, P.; Shah, N. A Multi-Objective Multi-Period Optimization of Carbon Integration Networks in Industrial Parks. In *Comput.-Aided Chem. Eng.*; Elsevier Masson SAS, 2019; Vol. *46*, pp 487−492.
(42) Fuentes-Cortés, L. F.; Serna-González, M.; Ponce-Ortega, J. M. Analysis of Carbon Policies in the Optimal Design of Domestic Cogeneration Systems Involving Biogas Consumption. *ACS Sustain. Chem. Eng.* **2017**, *5* (5), 4429−4442.
(43) Noureldin, M. M. B.; El-Halwagi, M. M. Synthesis of C-H-O Symbiosis Networks. *AIChE J.* **2015**, *61* (4), 1242−1262.
(44) Panu, M.; Topolski, K.; Abrash, S.; El-Halwagi, M. M. CO_2 Footprint Reduction via the Optimal Design of Carbon-Hydrogen-Oxygen SYmbiosis Networks (CHOSYNs). *Chem. Eng. Sci.* **2019**, *203*, 1−11.
(45) Allam, R.; Martin, S.; Forrest, B.; Fetvedt, J.; Lu, X.; Freed, D.; Brown, G. W.; Sasaki, T.; Itoh, M.; Manning, J. Demonstration of the Allam Cycle: An Update on the Development Status of a High Efficiency Supercritical Carbon Dioxide Power Process Employing Full Carbon Capture. *Energy Procedia* **2017**, *114*, 5948−5966.
(46) Medrano-García, J. D.; Ruiz-Femenia, R.; Caballero, J. A. Multi-Objective Optimization of Combined Synthesis Gas Reforming Technologies. *J. CO2 Util.* **2017**, *22*, 355−373.
(47) D'Angelo, S. C.; Mache, J.; Guillén-Gosálbez, G. Absolute Sustainability Assessment of Flue Gas Valorization to Ammonia and Synthetic Natural Gas. *ACS Sustain. Chem. Eng.* **2023**, *11* (50), 17718−17727.
(48) Woodcock, K. E.; Gottlieb, M. Gas, Natural. In *Kirk-Othmer Encyclopedia of Chemical Technology*; Wiley, 2004.
(49) Vázquez, D.; Guillén-Gosálbez, G. Process Design within Planetary Boundaries: Application to CO_2 Based Methanol Production. *Chem. Eng. Sci.* **2021**, *246*, 116891.
(50) González-Garay, A.; Frei, M. S.; Al-Qahtani, A.; Mondelli, C.; Guillén-Gosálbez, G.; Pérez-Ramírez, J. Plant-to-Planet Analysis of CO_2-Based Methanol Processes. *Energy Environ. Sci.* **2019**, *12* (12), 3425−3436.
(51) Lucas, T. R.; Ferreira, A. F.; Santos Pereira, R. B.; Alves, M. Hydrogen Production from the WindFloat Atlantic Offshore Wind Farm: A Techno-Economic Analysis. *Appl. Energy* **2022**, *310*, 118481.
(52) Medrano-García, J. D.; Charalambous, M. A.; Guillén-Gosálbez, G. Economic and Environmental Barriers of CO_2-Based Fischer−Tropsch Electro-Diesel. *ACS Sustain. Chem. Eng.* **2022**, *10* (36), 11751−11759.

https://doi.org/10.1021/acssuschemeng.4c06566
ACS Sustainable Chem. Eng. 2025, 13, 1473−1483

(53) Mesquita-Cunha, M.; Figueira, J. R.; Barbosa-Póvoa, A. P. New ε-Constraint Methods for Multi-Objective Integer Linear Programming: A Pareto Front Representation Approach. *Eur. J. Oper. Res.* **2023**, *306* (1), 286−307.
(54) Mavrotas, G. Effective Implementation of the ε-Constraint Method in Multi-Objective Mathematical Programming Problems. *Appl. Math. Comput.* **2009**, *213* (2), 455−465.
(55) Gavin, T.; Ray, S. *Chemical Engineering Design: Principles, Practice and Economics of Plant and Process Design*; Elsevier, 2012.
(56) Wernet, G.; Bauer, C.; Steubing, B.; Reinhard, J.; Moreno-Ruiz, E.; Weidema, B. The Ecoinvent Database Version 3 (Part I): Overview and Methodology. *Int. J. Life Cycle Assess.* **2016**, *21* (9), 1218−1230.
(57) Field, C. B.; Barros, V. R. *Climate Change 2014: Impacts, Adaptation, and Vulnerability Working Group II Contribution to the Fifth Assessment Report of the Intergovernmental Panel on Climate Change*; Cambridge University Press: New York, 2014.
(58) The MathWorks Inc. *MATLAB Version: 9.11.0 (R2021b)*; The MathWorks Inc.: Natick, Massachussetts, 2021. https://mathworks.com.
(59) Guimerà, R.; Reichardt, I.; Aguilar-Mogas, A.; Massucci, F. A.; Miranda, M.; Pallarès, J.; Sales-Pardo, M. A Bayesian Machine Scientist to Aid in the Solution of Challenging Scientific Problems. *Sci. Adv.* **2020**, *6* (5), eaav6971.
(60) Jog, S.; Vázquez, D.; Santos, L. F.; Caballero, J. A.; Guillén-Gosálbez, G. Hybrid Analytical Surrogate-Based Process Optimization via Bayesian Symbolic Regression. *Comput. Chem. Eng.* **2024**, *182*, 108563.
(61) Böhm, H.; Zauner, A.; Rosenfeld, D. C.; Tichler, R. Projecting Cost Development for Future Large-Scale Power-to-Gas Implementations by Scaling Effects. *Appl. Energy* **2020**, *264*, 114780.

https://doi.org/10.1021/acssuschemeng.4c06566
ACS Sustainable Chem. Eng. 2025, 13, 1473−1483